Broadband Monolithic Constrained Lens Design

by

Leonard Thomas Hall

B.E. (Electrical & Electronic, with Honours),
The University of Adelaide, Australia, 2000

Thesis submitted for the degree of

Doctor of Philosophy

in

School of Electrical and Electronic Engineering,
Faculty of Engineering, Computer and Mathematical Sciences
The University of Adelaide, Australia

August, 2009

Chapter 5

Contributions to Rotman Lens Theory

THE previous chapter introduced the Rotman equations in their standard form and described the three levels of analysis used to predict the performance of the Rotman lens. This chapter first rewrites the Rotman equations to suit the intended application of a feed network for a linear antenna array. It then uses these equations to examine the aberration performance of an ideal Rotman lens feed network.

An improved method of lens geometrical aberration characterisation is described that correctly separates beam pointing error, which does not degrade the beam-forming capability of the lens, from higher order errors that are responsible for increasing sidelobes and widening the main beam. This method is used to show how the parameter g, in the Rotman equations, is manipulated to minimise lens path length errors.

The new method of characterising geometrical aberration is then used to find the optimal focal arc for any set of Rotman variable values. This analysis demonstrates that the circular focal arc benefits very little from refocusing and is the best focal arc choice for the Rotman lens.

5.1 Normalisation by Aperture Size

The original Rotman lens path length equations were normalised by the focal length F. Although this approach is consistent with lens specifications in optics, and simplifies the solution to the path length equations, it means design studies involving the Rotman parameters result in different sized linear array apertures. As a multiple beam-forming network for a linear antenna array, it is convenient to rewrite these equations normalised by the size of the array aperture $2N_{\max}$.

The focal arc, lens contours and antenna aperture interrelationship for four lens geometries with different ratios of focal length, F, and aperture size, $2N_{\max}$, are illustrated in Figure 5.1. Figure 5.1(a) presents these four lenses using the standard form of the Rotman equations while Figure 5.1(b) shows the same four lens geometries scaled to drive an antenna aperture size of 1. The standard Rotman equations allow the size of the array aperture and lens contour to vary while the focal arc is kept fixed. In contrast, the renormalised equations allow the focal arc and beam port spacing to vary, while the lens contour remains approximately the same width and the array aperture is fixed.

The Rotman equations set the angular positions of the three perfect focal points to the angular direction of the excited wavefront. This limitation has been removed by varying the field-of-view independently to the angle of the three perfect focal points. This is achieved by scaling the dimensions of the lens without scaling the linear antenna array. The scaling factor is calculated as a trigonometric ratio of α, associated with focal points F_1 and F_2, and β, the angular offset of the resultant planar wave.

Consequently, Rotman designs presented in this thesis introduce two new parameters illustrated in Figure 5.2. The parameter f is introduced as the ratio of focal length to aperture size, and the variable β as the angular direction of the wavefront associated with the perfect focal point at α. The parameter F defined in terms of $N_{\max}$ becomes

$$F = 2fN_{\max}\frac{\sin(\beta)}{\sin(\alpha)}, \tag{5.1}$$

and n becomes

$$n = \frac{N}{2fN_{\max}}. \tag{5.2}$$

The condition that ensures real x and y is rewritten as

$$f \geq \min\left(0.5, \frac{1}{2n_1}, \frac{1}{2n_2}\right). \tag{5.3}$$

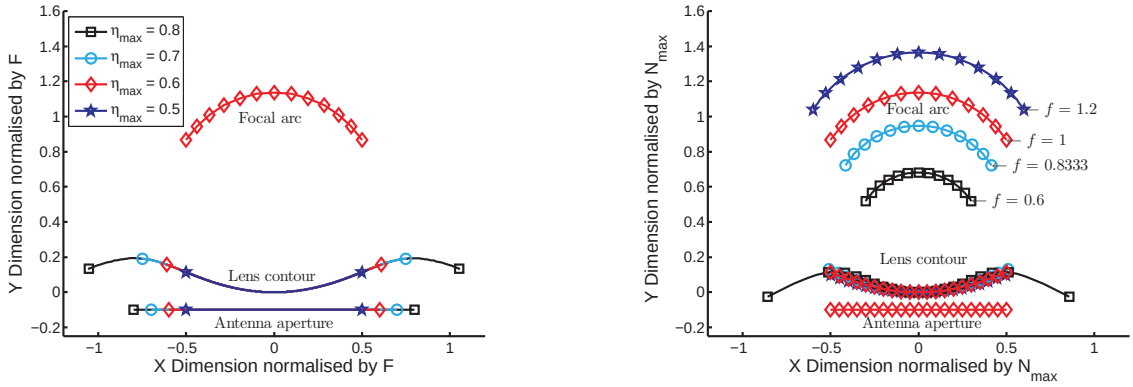

(a) Normalised by focal length.

(b) Normalised by aperture size.

Fig. 5.1: Lens renormalisation. The Rotman equations normalise the lens by the distance of the outer focal points to the origin of the lens. This approach causes the array aperture to vary with different choices of F, as shown in Subfigure (a). To compare the the performance of the different sets of Rotman parameters, the size of the array aperture should remain constant. To this end, the Rotman equations have been rewritten to normalise the lens by the length of the aperture. The result, shown in Subfigure (b), maintains constant aperture size and antenna element position for any set of Rotman parameters. Subfigure (a) shows four lenses with $2n_{\text{max}} = \frac{1}{1.2}, 1, \frac{1}{0.8}, \frac{1}{0.6}$, for $\alpha = 40°$, and $g = 1.2633$, while Subfigure (b) presents the equivalent lenses in the new Rotman equations with $f = 1.2, 1, 0.8333, 0.6$, $\alpha = 40°$, and $g = 1.2633$.

By redefining the variables F and n in this way, all lens dimensions are normalised by the size of the aperture. This formulation highlights the intended application of the Rotman equations and consequently the process of design and optimisation are greatly simplified.

5.2 Geometric Error Characterisation

The accepted wavefront aberration curve (Rotman and Turner 1963) results from two different error sources, beam pointing error and higher order error. Beam pointing or linear error does not undermine the beam pattern, but instead results in an angular offset of the beam and can be easily corrected by moving the beam port along the focal arc. Higher order errors are reduced by correctly refocusing the focal arc, but cannot be completely removed from the system and are the true limit of the theoretical lens performance. Figure 5.3 is a plot of normalised error as a function of aperture position, demonstrating that the linear offset caused by beam pointing error, plotted in blue, quickly

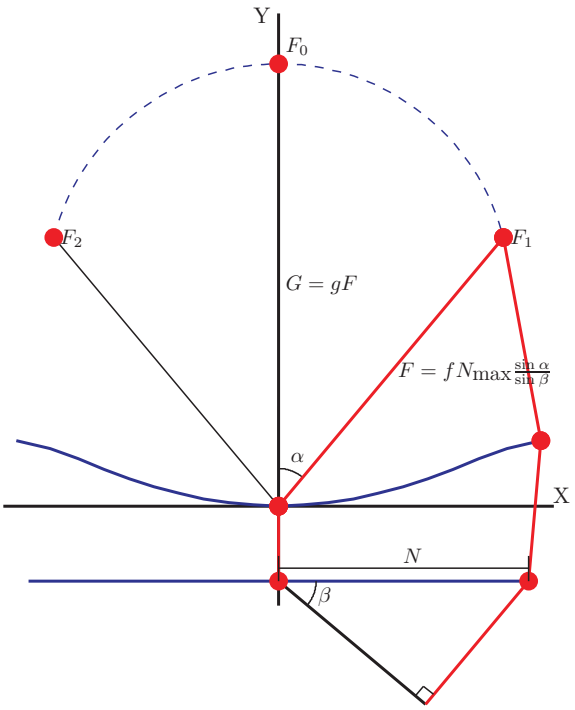

Figure 5.2: Renormalisation of Rotman equations. The renormalisation of the Rotman equations results in the new variable β to define the beam angle associated with the outer focal points, F_1 and F_2. The parameter F is now defined in terms of $N_{\max}$, α and β. This allows the antenna element spacing to be defined independently to the antenna port spacing.

dominates the higher order error in green. As a result, optimisation of the Rotman lens using the approach described by Rotman and Turner (1963), minimises pointing error rather than the higher order error.

To better represent lens errors, the path length error is redefined as the difference in path length between the linear wavefront and the realised wavefront at each antenna element. In contrast to the accepted definition described by Rotman and Turner (1963), no assumption of wavefront direction is made, and the errors are not renormalised by the focal length F.

To calculate the aberration of a single beam within a theoretical lens design, the path length between the desired beam port and each antenna element is calculated. The linear wavefront that minimises RMS path length error is then calculated and the remaining RMS path length error is taken as the beam port aberration performance. This procedure

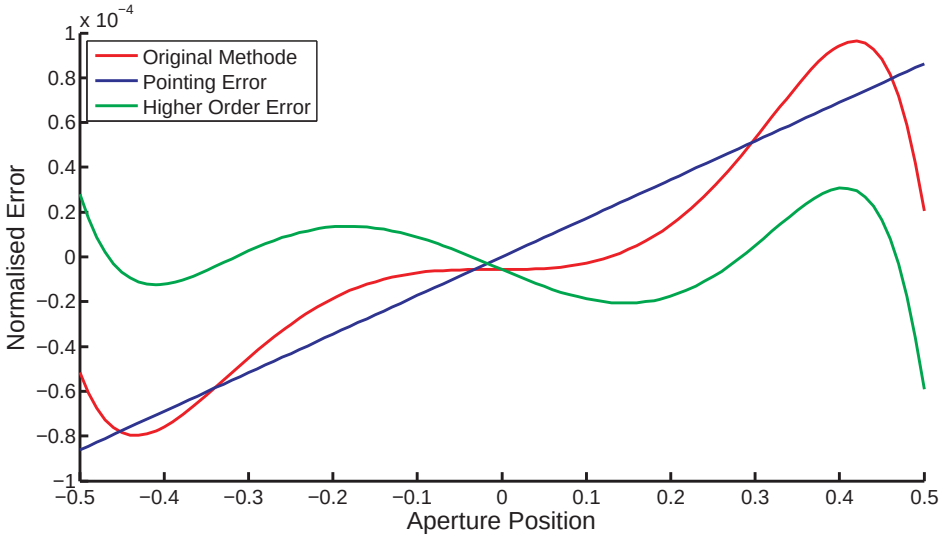

Figure 5.3: Path length error curves. The accepted definition of path length error includes a linear component that can be easily removed by moving the beam port along the focal arc. This linear error causes a shift in the angle of the beam, it does not reduce the gain or increase the sidelobes. The new definition of path length error is more appropriate because it recognises this effect. The new definition of path length error is separated into beam pointing error and RMS path length error.

is repeated for each beam port of the lens, the maximum RMS path length error within the field-of-view of the lens is referred to as the geometric error of the lens.

The path length errors are proportional to aperture size. For small apertures and wide beam widths, these errors are insignificant. As the desired aperture becomes larger, these errors become an important consideration of the lens design. The four parameters α, β, g and f not only define the shape of the lens contours, they also strongly effect aberrations.

5.2.1 Geometric Errors and Optimum g

The parameter g is chosen to minimise the aberrations for all beam port positions on the focal arc. Equations (4.21) and (4.22) have been suggested to calculate g that are reported to minimise the path length errors. However, little work has been carried out to substantiate this. Figure 5.4 plots the geometric error as a function of g for an aperture and focal length of 1 and $\alpha = \beta = 40°$. A clear minimum is present demonstrating that a simple gradient optimisation effectively finds the optimal value of g for any combination of $N_{\max}$, f, α and β.

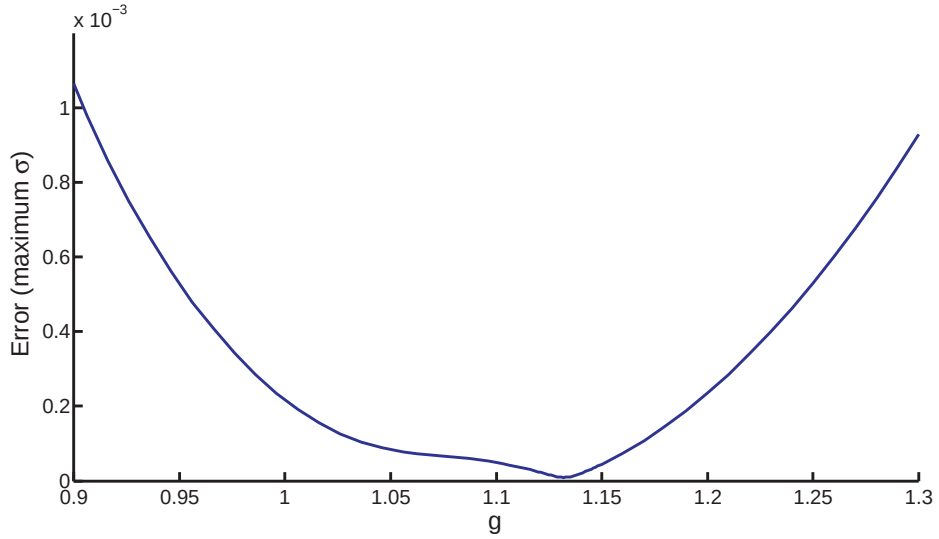

Figure 5.4: Aberrations and g. Discussion about the optimal choice of g have been popular in the literature. This figure shows the maximum RMS path length error, normalised to aperture length, for a range of g, $\alpha = 40°$ and $f = 1$. The figure shows that there is a single optimal value of g that can be found using a gradient optimiser.

To evaluate the accuracy of the two approximations for g, $g = 1 + \frac{\alpha^2}{2}$ made by Rotman and Turner (1963) and $g = 1/\cos(\alpha)$ made by Smith (1982), the optimal value for g has been found for a range of α and f. The optimum value of g is chosen to minimise the RMS path length error for a focal arc covering $\pm\alpha$. Figure 5.5(a) shows the value of g suggested by Rotman and Turner (1963) in red and by Smith (1982) in blue. These approximations are a function of α and independent of f. This results in only one line for each approximation. Figure 5.5(b) shows the optimal value of g for $0 \leq \alpha \leq 70$ and $f = 0.501, 0.6, 1, 2$. The optimal value for g closely follows the approximation suggested by Smith for $f \gg 1$. Rotman's approximation yields better results for $f \leq 1$ and $\alpha \leq 40°$.

For lens designs driving a small aperture, the lens aberrations are small and need not be optimised as both approximations yield acceptable results. Since most Rotman lenses are designed for limited field-of-view and compactness, the approximation suggested by Rotman will generally result in smaller errors.

When large apertures are being excited, the approximations are inadequate, causing degradation of the lens performance. Consequently, the optimal value of g should be found using numerical optimisation.

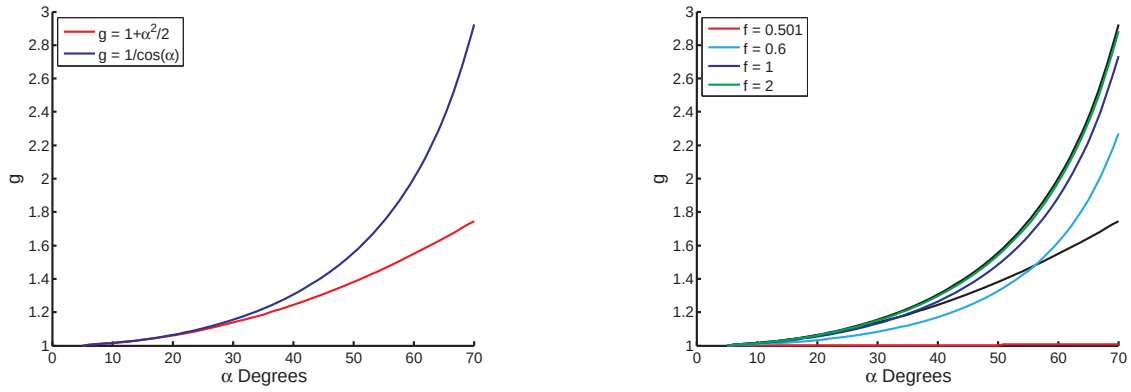

(a) Rotman in red, Turner and Smith in blue.

(b) Numerical optimisation of g.

Fig. 5.5: Estimate of optimal g. Subfigure (a) shows the value of g that Rotman and Turner (1963) and Smith (1982) suggested should be used, and Subfigure (b) compares these to the optimal value of g found using numerical optimisation. The optimal value of g converges on $1/\cos(\alpha)$, the value suggested by Smith, as $f >> 1$. As $f \rightarrow 0.5$ the optimal value of $g \rightarrow 1$. Since most practical implementations of a Rotman lens will choose $0.6 < f < 1$, numerical optimisation must be used to find the optimal value of g.

5.2.2 Geometric Errors Associated with f

The design parameter f is the normalised distance from the origin of the lens to the two off-axis focal points. Thus, f is effectively a scaling factor that varies the size of the Rotman lens relative to the aperture size. Figure 5.6(a) shows lens contours for different values of f, demonstrating that while the shape of the lens contour and focal arc remain constant, the portion of the lens contour that is utilised by the aperture is inversely proportional to f. By varying f, the lens contour and focal arc can be made to have similar widths. Although the antenna port spacings remain relatively constant, the beam port spacings vary considerably. Care must be taken to ensure that the port spacing allows enough space for practical port implementation. Figure 5.6(b) shows the normalised delay line length associated with each set of lens contours shown in Figure 5.6(a). While the lens contour is approximately circular, the delay line lengths remain small. As f is reduced the lenses curvature becomes stronger and the length of the outer delay lines increase.

Minimum f

The size of the lens is often required to be compact. Lens size can be reduced significantly by reducing the value of f. Practical lens geometries are achieved using values of f

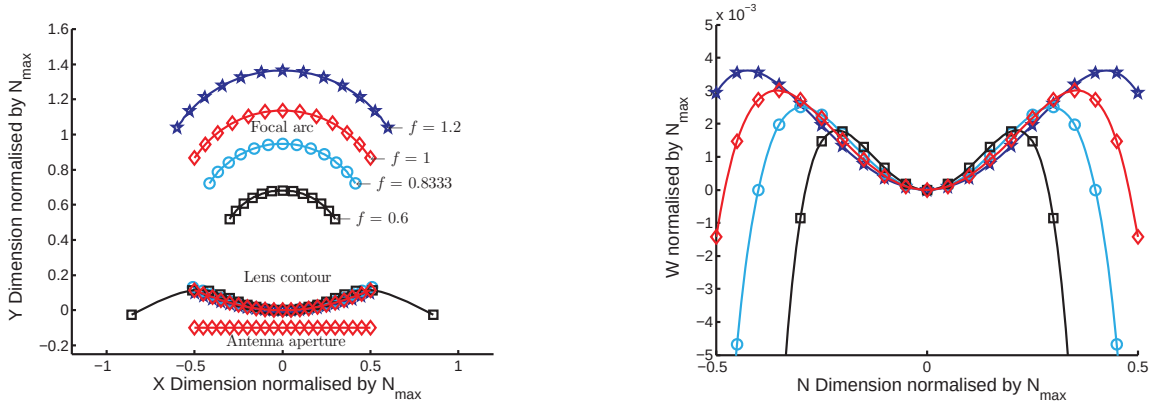

(a) Lens contour curves.

(b) Delay line lengths.

Fig. 5.6: Effect of parameter f. The variable f controls the size of the lens relative to the size of the aperture as seen in Subfigure (a). Subfigure (b) demonstrates that the length of the delay lines must be increased as the lens becomes smaller in response to the increased curvature of the array arc. These figures show the effect of varying f while $\alpha = 40°$, and $g = 1.2633$.

approaching that defined by Equation (5.3). Figure 5.7 plots the minimum value of f for a range of g and α. The most compact lens implementations should define the focal length to be one fourth the aperture size or $f = 0.5$. However design flexibility is limited since the parameter g must be kept close to unity for small values of α.

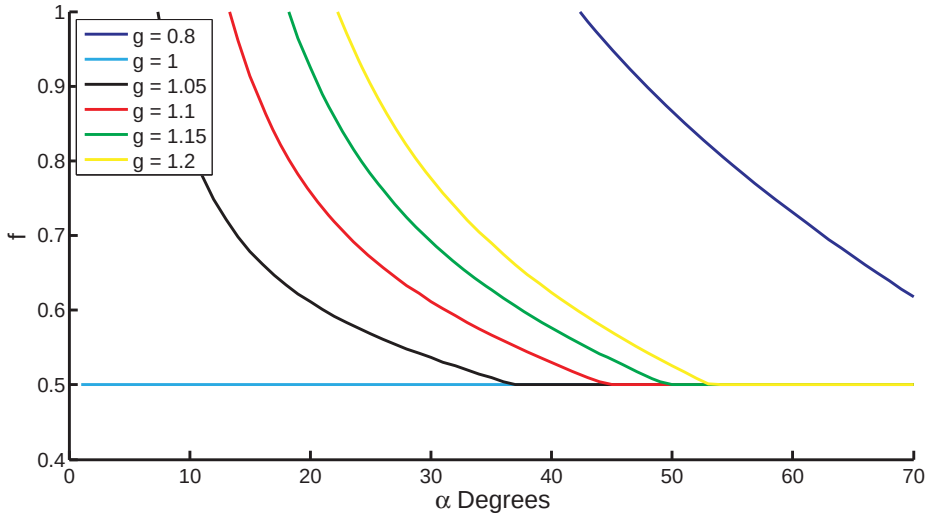

Figure 5.7: Minimum f. The length of the lens is minimised by choosing f to be small. The minimum value of f for which a solution to the Rotman equations exists, is shown in this figure for $g = 0.8, 1, 1.05, 1.1, 1.15, 1.2$. The length of the Rotman lens body can be reduced to approximately half the aperture width.

By making f small, path length errors are increased. The increasing error is a consequence of increasing n in the original equations. Figure 5.8 plots the worst case RMS path length error, for a range of f and $\alpha = 15°, 30°, 45°, 60°$ for a field-of-view of $\pm\alpha$, and shows that low errors are achieved in designs with narrow fields of view and where f is large.

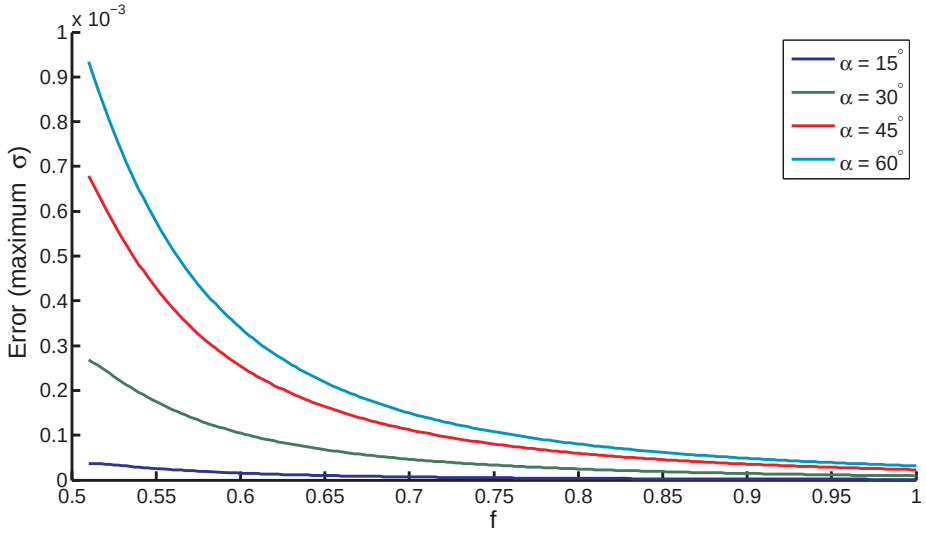

Figure 5.8: RMS path length error versus f. The error performance of the lens is inversely proportional to the variable f and therefore the size of the lens. This figure shows the minimum achievable error as f and α are varied, showing that errors are reduced as f becomes larger and α becomes smaller.

Care must be taken to ensure that the increased aberrations, as f is reduced, do not adversely effect the performance of the lens. Size reduction using this technique is only practical when the systems aberration requirements are relaxed.

5.2.3 Geometric Errors Associated with α, β and Beam Port Position

Although the original Rotman lens equations set the two angles, α and β, to be equal, the design equations become much more flexible when β is set to meet the field-of-view requirements and α is defined independently. Figure 5.9 shows lens contour diagrams for a typical lens design, $f = 1$, $g = 1.2$, $\beta = 40°$, and α is varied for a fixed field-of-view. Equation (5.1) shows that as α is reduced the distance between the outer focal points and the origin of the lenses is increased. Figure 5.9(a) shows that the focal arc width and beam port spacing remain almost constant. Unlike the beam port spacing, the antenna port spacing varies considerably. The difference between α and β is achieved by

varying the antenna port spacing along the lens contour while keeping the array element spacing constant. This results in more compact lenses with closely spaced antenna ports for large values of α, and larger lenses with widely spaced antenna ports for small values of α. Figure 5.9(b) shows the delay line lengths associated with the lens contours of Figure 5.9(a). As expected, the delay line lengths closely resemble the case where $\alpha = \beta$ shown in Figure 4.5.

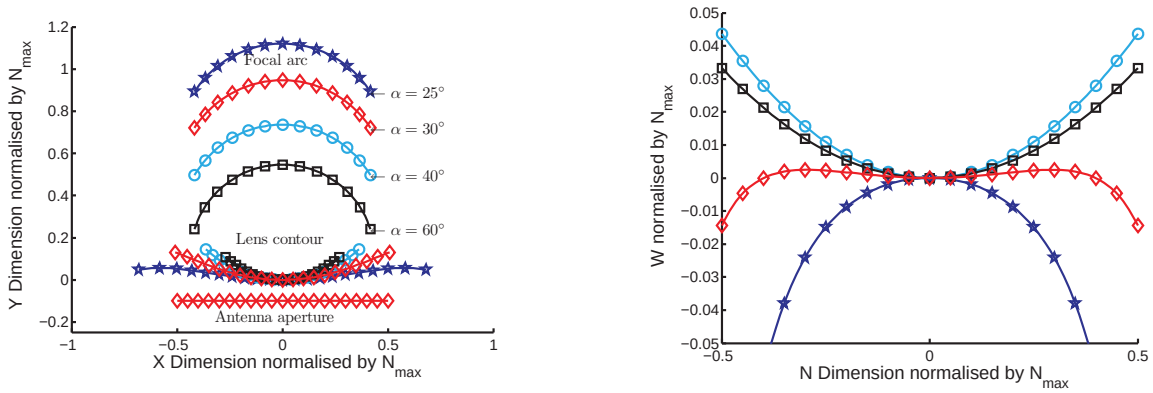

(a) Lens contour curves.

(b) Delay line lengths.

Fig. 5.9: Effect of parameter α. The variable α defines the angle between the central focal point and outer focal points. When α is varied while keeping β constant, the variable α also scales the size of the lens. This figure shows the effect of varying α on the lens contour and delay line lengths of the Rotman lens for $\alpha = 30°$, $40°$, $60°$, $f = 1$, and $g = 1.2633$ while keeping field-of-view constant, $\beta = 40°$. Both lens contour curves and delay line lengths are normalised by the aperture size.

The focal arc is assumed to be circular, joining the three focal points of the Rotman lens. The beam ports are placed at positions on this focal arc corresponding to the required beam angles. Figure 5.10(a) shows how the RMS path length error varies with beam angle, and the corresponding beam port position on the focal arc, for $\beta = \alpha$. The phase error versus beam angle show errors increase rapidly past α. For this reason, most Rotman lens implementations make α equal or only slightly less than the maximum scan angle required by the system (Rotman and Turner 1963).

The work so far has assumed that $\beta = \alpha$. By defining β independently there is more freedom to optimise the lens design. Figure 5.10(b) shows the RMS path length error as a function of beam angle for four lenses, $\alpha = 25°$, $30°$, $40°$, $60°$, while setting $\beta = 40°$. The error increases almost linearly as α becomes larger. This shows that by setting β

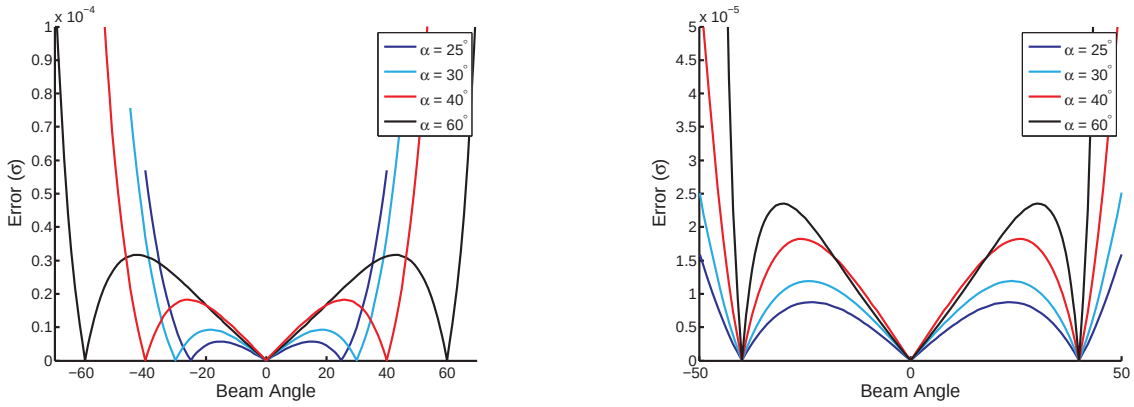

(a) $\alpha = \beta$ (b) Fixed $\beta = 40°$

Fig. 5.10: Relationship between aberrations, f and g. The error performance of each beam of the Rotman lens is effected by the beam angle and the variables α and β. Subfigure (a) demonstrates the relationship between beam angle and $\alpha = \beta$ while Subfigure (b) shows the relationship between beam angle and α while $\beta = 40°$.

to satisfy the field-of-view requirement of the lens, α may be varied to optimise the lens without substantial degradation of performance.

5.3 Alternate Focal Arc and Refocusing

Rotman and Turner (1963) assume a circular focal arc connecting the three perfect focal points, however other focal arcs have been used in the literature. Singhal et al. (1998), using parabolic, hyperbolic, elliptical and straight focal arcs, conclude that a lens designed using an elliptical focal arc is more compact compared to the circular focal arc lens, with comparable path length errors. Another approach used extensively in the design of dual focal point lenses is refocusing (Ruze 1950). Surprisingly, refocusing of the Rotman lens has attracted very little attention in the literature. A convincing argument has not been presented to suggest one focal arc design is superior to any other.

Refocusing the focal arc of the Rotman lens yields the focal arc exhibiting the minimum path length error and, by definition, the optimal focal arc. In this way, refocusing is used here to select the best focal arc approximation. Figure 5.11 shows the minimum achievable error using a refocused focal arc compared to a circular focal arc. The figure clearly shows that the circular focal arc results in the same optimal g as the refocused focal arc, at the same magnitude of error. Figures 5.11(a) and 5.11(b) show that small improvements in aberration performance can be achieved for field-of-view less than 30°.

However, the focal arc closely resembles the circular focal arc and does not substantially reduce size of the lens.

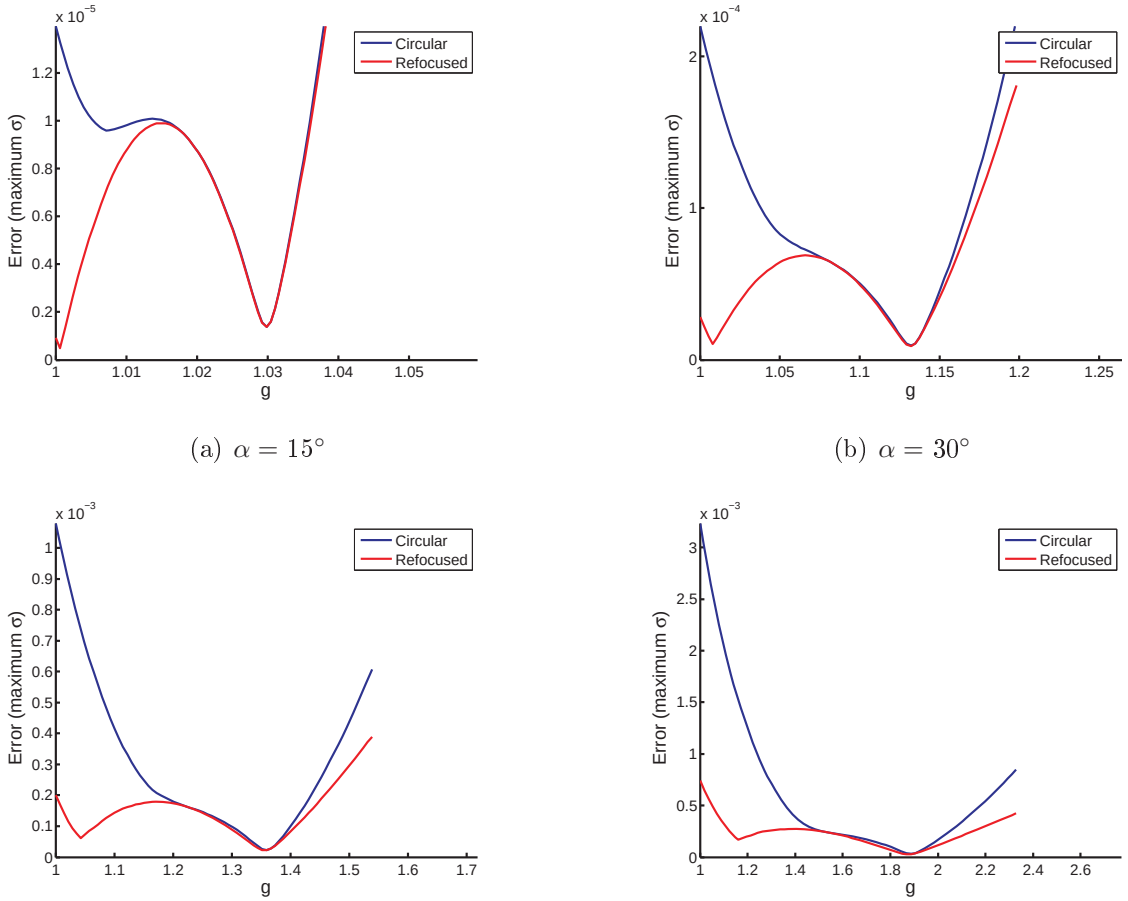

(a) $\alpha = 15°$ (b) $\alpha = 30°$

(c) $\alpha = 45°$ (d) $\alpha = 60°$

Fig. 5.11: Aberration performance of circular and refocused focal arcs. The minimum phase error cannot be improved significantly by refocusing of the focal arc. The size of the lens can be reduced by selecting the second local minimum of the refocused focal arc. These figures show the relationship between the normalised worst case RMS path length error at any point on the focal arc for the circular and optimised focal arc. These plots show the additional local minimum at a lower g for the optimised focal arc

Figures 5.11(c) and 5.11(d) show that for large fields of view, the second local minima in path length error as a function of g remains. Figure 5.12(a) demonstrates the refocused focal arc compared to the circular focal arc design. The refocused focal arc does not resemble any of the alternate focal arcs suggested in the literature. Although the errors are slightly greater than that of the optimal circular focal arc, the value of g is reduced significantly resulting in a more compact lens. The position of the second local minima

for the refocused lens is shown in Figure 5.12(b) compared to the optimal g and the approximations for g made by Rotman and Turner (1963) and Smith (1982).

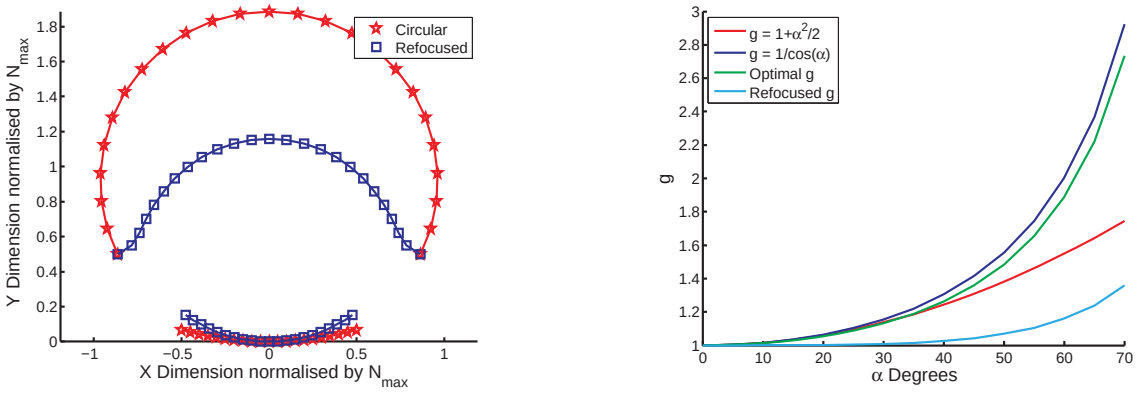

(a) Lens contour curves.

(b) Choice of g.

Fig. 5.12: Refocused Rotman lens size reduction. Refocusing of the focal arc allows smaller values of g to be used without substantial increases in phase error. This is clearly seen in Subfigure (a) showing the optimal circular and optimal refocused focal arc for $\alpha = 60°$. Subfigure (b) shows the estimate of optimal values of g suggested by Rotman and Turner (1963) and Smith (1982), and optimal values of g found using optimisation of circular focal arc and optimised focal arc.

There are two choices when selecting the best focal arc for the Rotman lens, the circular focal arc or the refocused focal arc. The circular focal arc results in the smallest errors and is easy to implement. If size constraints or other limitations make the circular focal arc unsuitable, the refocused focal arc has comparable performance resulting in a more compact lens. The difficulty and computation time involved in optimising the value of g for the Rotman lens using a refocused focal arc makes this option unattractive.

5.3.1 Symmetric Rotman Lens

The symmetric Rotman lens connects the three focal points with a reflection of the lens contour. The front-to-back symmetry makes this Rotman lens implementation ideal for reflection-based lenses and applications requiring focusing in both directions. The symmetrical Rotman lens is also claimed to have a number of performance advantages over standard Rotman lens designs.

To compare the performance of the symmetrical Rotman lens to the asymmetric lens a set of equations expressing g, α and n in terms of A and C, must be defined. Following

this an error analysis of the symmetrical Rotman lens is performed in the same way as the asymmetrical lens.

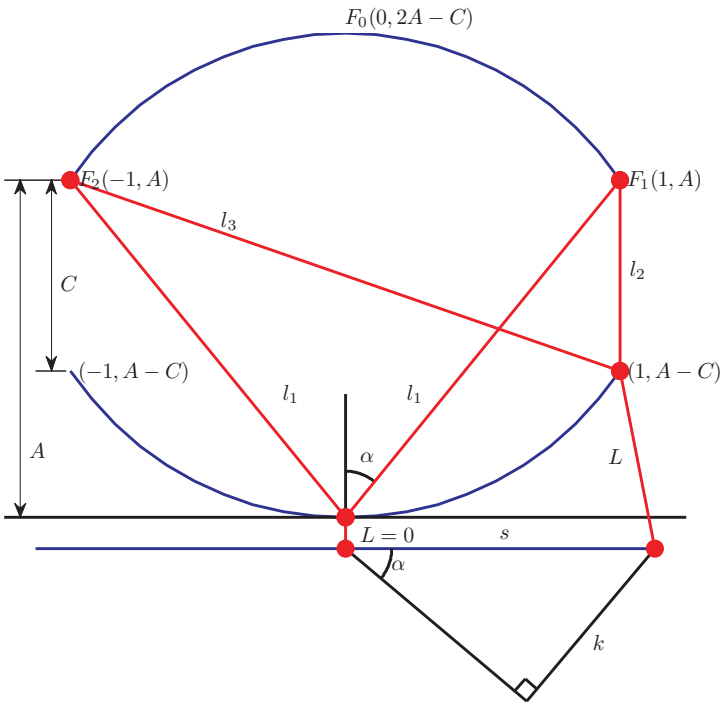

Figure 5.13: Symmetrical Rotman lens geometry. The symmetrical Rotman lens replaces the focal arc with a mirrored array arc. The symmetrical Rotman lens equations are based on the two variables A and C. For the first time, these variables are related to the Rotman variables F, G, and α. This has allowed the performance of the symmetrical Rotman lens to be compared to the standard Rotman lens.

Derivation of Equations

Using a similar approach to Shelton and Kelleher (1961), equations defining g and f in terms of α can be found. From Figure 5.13, we can write the equations that collimate the wavefronts from the two off-axis focal points:

$$l_1 = l_2 + L + k, \tag{5.4}$$

$$l_1 = l_3 + L - k. \tag{5.5}$$

By subtracting Equation (5.5) from Equation (5.4)

$$0 = l_2 - l_3 + 2k,$$

$$k = \frac{1}{2}(l_3 - l_2). \tag{5.6}$$

Expressions for the path lengths are:

$$\begin{aligned} l_2 &= C, && (5.7)\\ l_3 &= \sqrt{(A-(A-C))^2+2^2}, \\ &= \sqrt{C^2+4}. && (5.8) \end{aligned}$$

Combining Equations (5.7) and (5.8) with Equation (5.6) gives

$$k = \frac{1}{2}(\sqrt{C^2+4}-C).$$

The wavefront originating from F_1 should leave the aperture at an angle α. The length of the aperture can then be found from:

$$\begin{aligned} \frac{k}{s} &= \sin(\alpha) = \frac{1}{\sqrt{A^2+1}}, \\ s &= k\sqrt{A^2+1}. \end{aligned}$$

From Figure 5.13, $G = 2A - C$ and $F = \sqrt{1+A^2}$ therefore

$$\begin{aligned} g &= \frac{G}{F}, \\ &= \frac{2A-C}{\sqrt{1+A^2}}. \end{aligned}$$

Also from Figure 5.13 the aperture size is $2s$ therefore

$$\begin{aligned} f &= \frac{F}{2s}, \\ &= \frac{\sqrt{1+A^2}}{2k\sqrt{A^2+1}}, \\ &= \frac{1}{2k}, \\ &= \frac{1}{\sqrt{C^2+4}-C}. \end{aligned}$$

Shelton's equations connecting the two variables A and C are

$$A = \cot(2\arctan\left(\frac{1}{2}\tan\left(\frac{1}{2}\operatorname{arccot}\left(\frac{C}{2}\right)\right)\right)), \text{ and} \quad (5.9)$$

$$C = 2\cot(2\arctan\left(2\tan\left(\frac{1}{2}\operatorname{arccot}(A)\right)\right)). \quad (5.10)$$

Now, $A = \cot(\alpha)$ and $\alpha = \operatorname{arccot}(A)$ therefore Equations (5.9) and (5.10) become

$$\begin{aligned} \alpha &= 2\arctan(\frac{1}{2}\tan\left(\frac{1}{2}\operatorname{arccot}\left(\frac{C}{2}\right)\right)), \\ C &= 2\cot(2\arctan\left(2\tan\left(\frac{\alpha}{2}\right)\right)). \end{aligned}$$

The design equations for the symmetrical Rotman lens based on the single parameter α becomes:

$$\begin{aligned} A &= \cot(\alpha), \\ C &= 2\cot(2\arctan\left(2\tan\left(\frac{\alpha}{2}\right)\right)), \\ g &= \frac{2A - C}{\sqrt{1 + A^2}}, \\ f &= \frac{1}{\sqrt{C^2 + 4} - C}. \end{aligned} \tag{5.11}$$

The case for $C = 0$ yields the most compact solution to the Rotman equations:

$$\begin{aligned} \alpha &= 2\arctan(\frac{1}{2}), \\ &\approx 53.13^\circ, \\ f &= 0.5, \\ g &= 1.2. \end{aligned}$$

Size and Errors

While the width of the lens remains reasonably constant, the depth of the lens varies considerably with α. The lens contour curves shown in Figure 5.14(a) indicate that the lens becomes larger as α is decreased, making the symmetrical lens impractically large for narrow fields of view. Another important feature is that the focal arc and lens contour remain approximately circular. Figure 5.14(b) shows that while the lens contours change significantly, the lengths of the delay lines vary only slightly.

The design equations presented above define the parameters f and g from the single variable α. Figure 5.15 shows how these variables change with α and compare them with the values of g suggested by Rotman and Turner (1963) and Smith (1982) and the optimal value of g found using the method described in Section 5.2. The curve for optimal g does not resemble that from Figure 5.5(b) because the value of f is also changing. The optimal g becomes equal to the symmetrical case as $\alpha \to 53.13^\circ$.

Unlike the circular focal arc, the symmetrical lens cannot easily correct beam pointing error. This is because the position of the beam ports are the same for that of the antenna ports. To correct beam pointing error, the position of the beam port is moved along the focal arc, in the case of the symmetrical lens, this results in nonuniform spacing of the antenna elements. The worst case beam offset is shown in Figure 5.16(a). For small

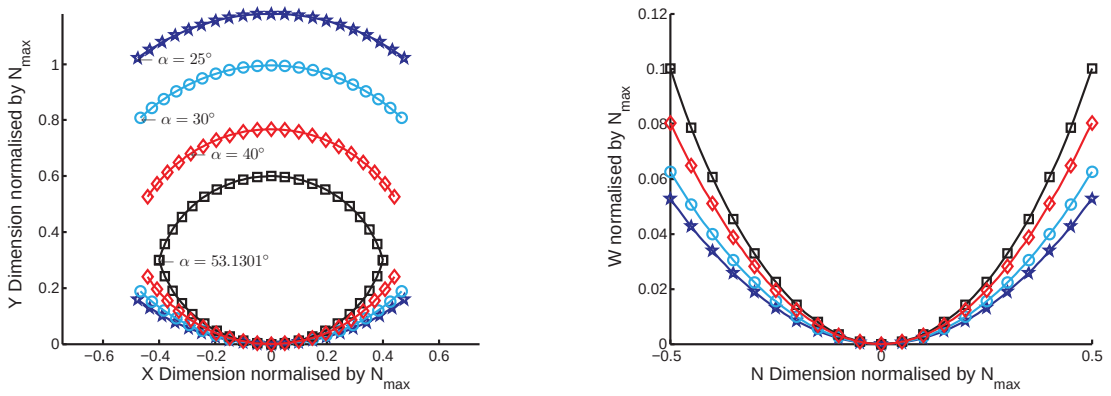

(a) Lens contour curves.

(b) Delay line lengths.

Fig. 5.14: Effect of parameter α on symmetrical lens. The symmetrical Rotman lens closely resembles a Rotman lens with a circular focal arc. The position of each beam port must mirror the antenna port so beam pointing errors can no longer be corrected. If the lens contour is allowed to extend past the outer focal points, aberrations increase significantly in the same way they do for the standard Rotman lens.

aperture sizes the beam pointing error is small, however for applications requiring narrow beams and large field-of-view, the beam pointing error becomes significant.

The remaining error, measured by the maximum standard deviation of the wavefront from the ideal planar wave, is shown in Figure 5.16(b). The errors are significantly larger than what is achievable using a circular focal arc. As $\alpha \rightarrow 53.13°$ the errors become identical. Figure 5.16(a) also shows the error performance of the circular focal arc using the same f, g, and α as the symmetrical lens. The error performance of the two is almost identical.

The equation for f assumes that the lens contour and focal arc do not extend past the outer focal points. By choosing f to be smaller than the value defined by Equation (5.11), the lens contour continues past the focal points F_1 and F_2. Larger values truncate the focal arc before it reaches the outer focal points. Figure 5.17(a) demonstrates how the parameter f effects the symmetric Rotman lens geometry. Figure 5.17(b) shows that while f is kept less than Equation (5.11), the error remains very similar for symmetrical and asymmetrical lens designs. The error performance is significantly degraded by using the symmetrical lens if the focal arc extends beyond the outer focal points when compared to an equivalent circular focal arc. In all cases the optimised circular focal arc displays improved aberration performance. These trends are seen for all values of α.

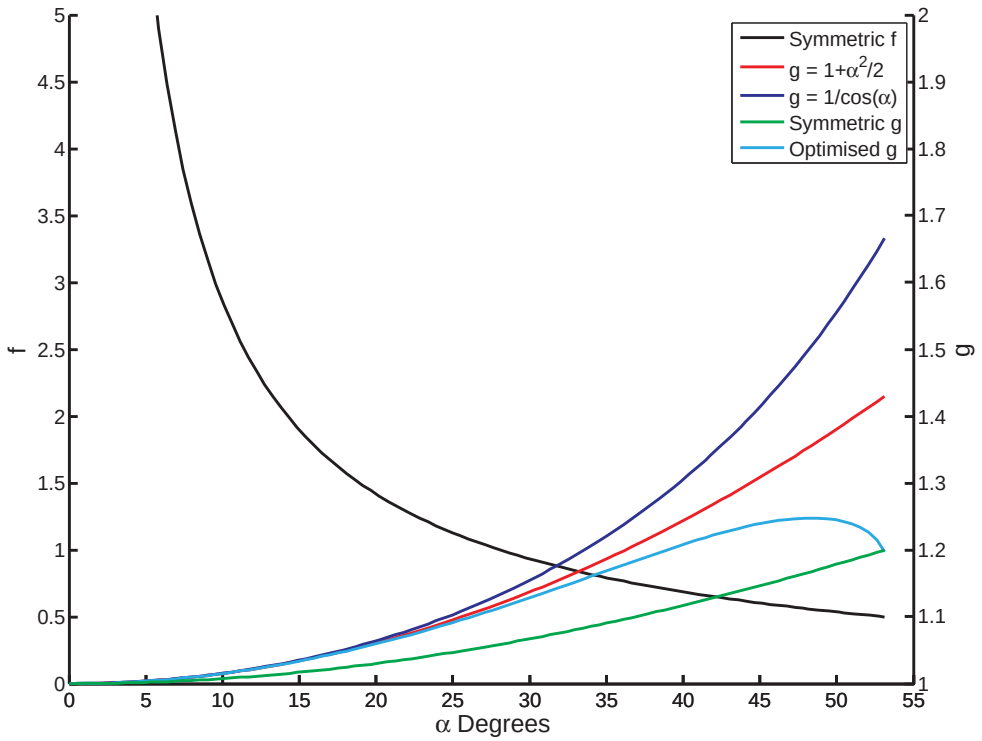

Figure 5.15: Symmetrical and non-symmetrical lens parameters. This figure shows the relationship between the Rotman variables of the symmetrical Rotman lens. This is compared to the optimal g of the circular and optimal refocused focal arc. The values of g suggested by Rotman and Turner (1963), $g = 1 + \frac{\alpha^2}{2}$, and Smith (1982), $g = 1/\cos(\alpha)$, are also shown.

Shelton and Kelleher (1961) suggests six reasons for choosing the symmetric configuration over the asymmetric lens. Because the design equations for the symmetric lens described by Shelton are so different from the original Rotman lens equations, a comparison of the two approaches is difficult. Using the design equations presented in Section 5.3.1 we can see that the focal arc of any symmetrical lens can be replaced with a circular focal arc resulting in a lens of equal size. As the focal arc for the symmetrical lens is very close to circular, the equivalent circular focal arc is almost indistinguishable from the symmetrical arc.

The symmetrical Rotman lens has few advantages over standard Rotman lens topologies. The symmetrical topology is ideally suited to reflection based and reversible lens implementations Shelton and Kelleher (1961). The symmetrical lens equations define values for

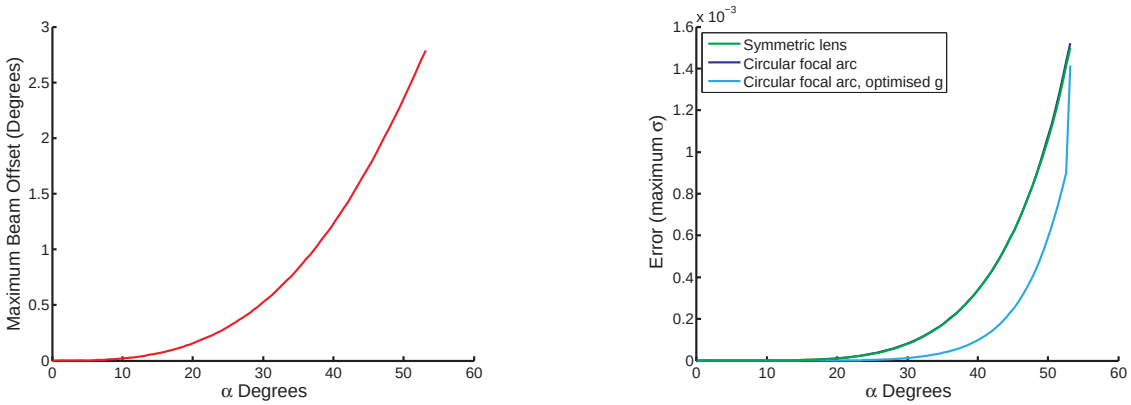

(a) Pointing error.

(b) RMS phase error.

Fig. 5.16: Symmetrical focal arc performance comparison. This figure shows the performance of symmetrical Rotman lens compared to circular focal arc and circular focal arc with optimal g. Subfigure (b) clearly shows that the performance of the the non-symmetrical Rotman lens is superior while replacing the symmetrical focal arc with a circular focal arc achieves similar RMS path length error without the pointing error shown in Subfigure (a).

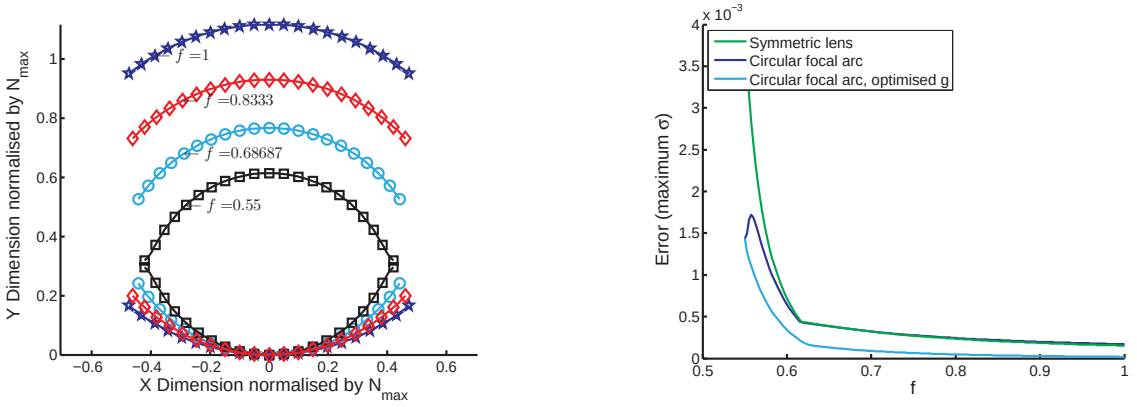

(a) Lens contour curves.

(b) Aberration performance.

Fig. 5.17: Effect of f and aberrations. As the symmetrical Rotman lens contour is allowed to increase beyond the outer focal points, $f < 1$, the magnitude of the phase aberrations increase quickly. Subfigure (a) demonstrates how the area of the lens body is reduced as the outer beam ports and antenna ports are drawn closer together. Subfigure (b) clearly shows that the standard Rotman lens, shown in light blue, performs better under all conditions.

f and g where the focal arc and lens contour have identical lengths. This may be useful in many lens designs as a starting point.

5.4 Chapter Summary

There are many claims in the literature that focal arcs other than the circular solution offer improved performance and more compact lenses. By finding the optimal focal arc numerically, for a large range of f, g, and α, results have been compared to the circular focal arc and symmetrical lens design. This comparison revealed that path length error improvements are insignificant when the circular focal arc is replaced with the optimal focal arc. The presence of a second minima in error using the refocused lens does allow a more compact lens to be implemented. This is especially advantageous for large values of α where the circular focal arc requires large g to minimise errors. The only other focal arc implementation of merit is the symmetrical focal arc. The symmetrical topology is ideally suited to reflection based and reversible lens implementations, but is of little use for general lens applications.

This chapter has rewritten the Rotman equations to reflect that the requirements of a Rotman lens are set by the requirements of the antenna array it drives. To this end two new variables have been introduced, f, the ratio of focal length to array aperture size, and β, the beam angle associated with the perfect focal point at angle α. Illustrative examples were then used to demonstrate how each parameter effects the Rotman lens geometry.

The need for a rigorous method of measuring Rotman lens aberration has been highlighted. The practise of measuring normalised path length error referenced to the linear wavefront that minimises the RMS path length error, is a significant improvement over the currently accepted method of using the maximum path length deviation from the theoretical linear wavefront. Using this technique, the influence of the Rotman parameters on the aberration performance has been clarified.

The error analysis revealed the existence of an optimal value of g. This allows aberrations to be minimised for a circular focal arc. The analysis shows that the approximation by Smith (1982) is very close to the optimal value of g for large values of f. Both approximations of g made by Rotman and Turner (1963) and Smith (1982) can be used for lens designs with relaxed error requirements.

The discussion surrounding the selection of an optimal focal arc has been addressed. Refocusing has been used to show that the Rotman lens constructed using an optimised

circular focal arc yields lower aberrations than any other focal arc approximation suggested in the literature. This analysis also shows that a more compact Rotman lens is achievable using a refocused focal arc, without a substantial increase in aberrations.

Comparing the symmetric and asymmetric Rotman lens geometries is made difficult because the equations describing the symmetric and asymmetric Rotman lens geometries are based on very different variables. The asymmetric lens equations have been rewritten based on the single parameter α. To simplify the comparison between the two lens topologies, equations have also been derived for g and f. Performance analysis of the symmetric and asymmetric Rotman lens geometries have been provided.

Chapter 7 applies these insights to the practical implementation of three Rotman lenses. Before this can be attempted, an assortment of tools must be chosen or, if nothing satisfactory is available, tools must be created. Further a set of measurement standards should be defined so that the Rotman lens performance may be judged. The following chapter presents the chosen software tools and the measurement standards used to evaluate the performance of the Rotman lenses presented in this thesis.

Chapter 6

Methods

THIS chapter presents the software tools, equipment, and methods used to design, simulate, and measure the performance of the constrained lenses presented in this thesis. The chapter begins with the software packages used to design and simulate these lenses. The equipment and procedure used to measure the realised lens designs are then described. The lenses are tested against a number of performance measures. These are explained in detail and the procedures used to evaluate them are described.

6.1 Software Tools

6.1.1 Numerical Analysis and Layout

The production of our first Rotman lens used Protel (Altium 2002) for the layout and each microstrip line was entered manually. Manual layout greatly limited the lens complexity and size. The designs implemented in this way were simplistic, even naive. However, they did highlight the need for an automated layout facility and a more rigorous design methodology.

A number of software tools are available to automate the layout of microstrip lines and the body of the lens. The approach taken in this thesis is to use Matlab to generate a simple two dimensional layout tool that is able to export this layout in DXF (Autodesk 1992) or GERBER (Buchanan 1996) file format for use in any number of simulators or for manufacture. The advantage of this approach is that Matlab is also able to calculate and display the performance of the design using both the geometrical optics model described in Section 4.2 and the two dimensional aperture model in Section 4.3.1. Results of electromagnetic simulation has been integrated into the layout tool for the design of the many matching networks and antenna elements used in these designs. In this way Matlab has been used to create a design environment that could accommodate the growing complexity of lens designs.

6.1.2 Electromagnetic Simulator Packages

Electromagnetic field solvers provide the means to look inside a structure and display surface currents, various electric and magnetic field plots or other quantities derived from the fields. Visualisation capabilities are built into most field solvers, which can lead to new insights into how RF and high speed digital components behave.

While significant work has been carried out in the literature on the design of boundary integral method (BEM) solvers for the design of Rotman lenses, the development of an electromagnetic simulation package is a very time consuming process. The availability of commercial electromagnetic simulation packages provides access to quick and highly accurate EM models without this significant investment in time.

What follows is a brief description of numerical methods that are used to treat Maxwell's equations and examples of the popular software packages that use them. Based on this

brief overview the reasoning behind the choice of electromagnetic simulation packages used in the lens designs described in Chapter 7.

Classification by Solution Domain

Electromagnetic field solvers are generally grouped according to the types of geometries they solve and the method used to simplify Maxwell's equations. Moreover, three dimensional arbitrary field solvers such as CST, Optimal O-Wave, HFSS, and Microstripes can be divided into three solution domain categories:

- frequency domain,
- time domain and
- eigenmode or modal solvers.

Frequency domain solvers generally solve Maxwell's equations in their integral form. The problem is divided into small segments and represented in matrix form that is then solved iteratively, or using matrix inversion. This process is repeated for each frequency point resulting in long simulation times for broadband or fine frequency resolution simulations. This is improved using a *fast sweep* option that is based on finding a rational polynomial that describes the solution behavior using a minimum set of computed frequency points (Hazdra et al. 2005). The numerical method used in these simulators is typically Method of Moments (MoM) (Harrington 1968, Burke and Poggio 1981), Finite Element Method (FEM) (Silvester 1973, Silvester and Ferrari 1996), or Spectral Domain Method (SDM) (Mosig 1989).

Popular frequency domain simulators are:

- Zeland IE3D (Zeland Software 2008b),
- Ansoft HFSS (Ansoft 2008b),
- Ansoft Designer (Ansoft 2008a),
- FEKO (Feko 2008),
- SuperNEC (Poynting Software 2008),
- Momentum-ADS (Agilent Technologies 2008),

- EMSight-AWR (AWR 2008), and
- Sonnet Suite (Sonnet Software 2008b).

Time domain solvers generally solve Maxwell's equations in their differential form. After the problem has been divided into small segments, the structure is excited by a time domain waveform and the field quantities of each segment are varied until convergence is reached. The time domain response is then easily converted to the frequency domain using the discrete or fast Fourier transform over the desired band. Structures that are highly resonant or have many ports or excitations are slow to simulate in the time domain. Typical methods are Finite Difference Time Domain (FDTD) (Yee 1966), Finite Integration Technique (FIT) (Computer Simulation Technology 2008), and Transmission Line Matrix (TLM) method (Johns and Beurle 1971, Hoefer 1989).

Popular time domain simulators are:

- CST Microwave Studio (Sonnet Software 2008a),
- Semcad (Semcad 2008),
- IMST Empire (IMST 2008),
- Fidelity (Zeland Software 2008a),
- QuickWave (QWED 2008),
- Mefisto (FAUSTUS Scientific Corporation 2008), and
- MicroStripes (Flomerics 2008).

Eigenmode or modal solvers calculate the eigennumbers and eigenmodes of the problem's homogenous wave equation. This is usually the choice for modelling of resonators, however two dimensional modal analysis is widely used to calculate and identify supported modes of transmission lines. Eigenmode solvers are included in Ansoft HFSS, FEMLAB and CST Microwave Studio.

Classification by Geometry

Electromagnetic simulation packages are also classified by the number of independent space variables or dimensions on which the field and source functions are dependent. By

simplifying a three dimensional model to a two dimensional problem, the solution accuracy in increased or the computational expense is decreased. Consequently much larger and complex problems may be solved when compared to a three dimensional solver.

Single dimensional methods are used for solving problems where the field and source functions depend on one space dimensions only. Typical examples are transmission line problems, uniform plane wave propagation or spherically or cylindrically symmetrical problems with only radial dependence.

Two dimensional methods are used for solving problems where the fields and source functions depend on two dimensions. Typical applications are planar structures, such as transmission line cross section problems, where the method is used to calculate the transmission lines characteristic impedance and propagation constant.

Three dimensional planar or 2.5D methods are used to solve problems with three dimensional fields, while the sources and currents are mainly confined to conductive planes with two dimensions. These problems tend to consist of a number of dielectric layers with arbitrary planar conductive geometries between them. These simulators are generally closed boundary MoM or open boundary MoM. The closed-boundary method uses a uniform rectangular mesh and a fast Fourier transform based solution method. This approach leads to very fast and accurate solutions, for problems in correctly meshed conductive boxes. This method is less effective for problems with curved surfaces or that require angled ports. While the open boundary method is slower, it assumes the structure is unshielded, or in a free space environment, and often uses triangular meshing to represent curved edges and angled ports.

Three dimensional methods are used for solving problems where fields, sources and currents vary in three dimensions. This category includes all volumetric full-wave general-purpose formulations. While these are able to solve any conceivable structure, they are the most computationally inefficient and as a result they are generally restricted to relatively small problems.

Electromagnetic Simulator Selection

For the purposes of this work, three problems must be solved using an electromagnetic simulation software package. The microstrip based lens designs, the port to lens interface, and various transmission line geometries must all be modelled.

The microstrip based constrained lenses, described in Section 7.5, are a two dimensional planar structure. Although it is the largest and most computationally expensive task, it is relatively simple with the correct software choice. Not all 2.5D frequency domain packages are appropriate for this task. The need to accurately represent angled ports restricts the choice to an open boundary MoM simulator. Ansoft Designer (Ansoft 2008a) meets these requirements and has been used to predict the scattering parameters for all lens simulations.

A simple 2.5D simulator is not convenient for the task of exploring the port to parallel plate interface described in Section 7.1. HFSS has been chosen for this task because of its tight control of boundary conditions, excellent visualisation capabilities and flexibility at the expense of model complexity and simulation time (Ansoft 2008b).

The large number of transmission lines used in Section 7.5 require a fast two dimensional eigenmode method. While HFSS is much better known for its FEM three dimensional simulation capability, its *ports only* solution is perfect for this task (Ansoft 2008b).

6.2 Lens Construction

The production of transmission line circuits, at millimetre wave frequencies, must be done carefully to ensure that lens performance is not degraded. The characteristic impedance of microstrip transmission line is dependent on the substrate height, dielectric constant and the width of the line. Substrate height and dielectric constant are controlled by the choice of the substrate manufacturer and substrate type. The accuracy of the microstrip transmission line impedance is dependent on the process tolerances of the printed circuit board manufacturer.

The important parameters defining quality of workmanship are minimum track width, minimum track spacing, plating thickness, and alignment tolerance of the upper and lower layers. The lens designs presented in this thesis are produced by Lintek Pty Ltd. Lintek's standard process uses a plating thickness of 35 μm and is able to achieve a track width tolerance of $\pm 12\,\mu$m and minimum width of 200 μm.

The substrate chosen for the microstrip constrained lenses designed in this thesis, is RT/Duroid 5870 supplied by the Rogers Corporation. This material is attractive due to the low dielectric constant, $\epsilon_r = 2.20$, that increases the transmission line width compared to higher dielectric constants, the low dissipation factor, $\tan\delta = 0.0009$ at 10 GHz, to

keep dielectric losses to a minimum, and the availability of thicknesses of 127 μm, 254 μm, 381 μm, 508 μm, and 787 μm. All lenses have been built using the dielectric thickness of 787 μm allowing a three fold increase in operation frequency by scaling the design.

The first two lenses described in Section 7.5.1 implement the dummy port loads using a 25 Ω/square thin film impedance called Ohmega-Ply (Ohmega 2008). Ohmega-Ply is a laminated thin foil of NiCrAlSi and comes in standard impedances of 10, 25, 50, 100, and 250 Ω/square. The thin film terminations are added to the lens at the expense of two additional process steps. Unfortunately the additional chemicals are difficult to dispose of in an environmentally friendly manner and Lintek has ceased using this process.

The broadband lens described in Section 7.5.2 has replaced the Ohmega-Ply with screen printed carbon polymer thick film ink called Electrodag PR-406. This material has an impedance of $< 10\,\Omega$/square and due to the inaccuracy of screen printing may suffer alignment errors up to 200 μm.

6.3 Lens Characterisation

The performance of lens described in Section 7.5.2 is completely described by the S-parameters measured using a vector network analyser (VNA). However, the two lenses described in Section 7.5.1 use integrated antenna elements that deny access to the antenna ports. In this case the combination of beam pattern and the S-parameter measurements must be used to judge the performance.

6.3.1 S-Parameters Measurement

The S-parameters are measured using a vector network analyser. The VNA measures the voltage magnitude of the reflected and transmitted signals compared to the incident signal. Therefore, a properly calibrated two port vector network analyser directly measures the values of the two port scattering parameters described in Section 3.2.2. The Rotman lens presented in Section 7.5.2 is a 16 port device, therefore it cannot be characterised by a single two port measurement. Instead, many measurements must be combined to construct the 16 port S-parameters.

The 16 element Rotman lens is characterised by measuring each element of the 16 port S-parameters separately. The S-parameters have 256 elements relating the incident, reflected, and coupled energy between any two ports. The procedure used to measure the 16

port Rotman lens makes use of the property that S-parameters are measured with a 50 Ω load connected to each port. By placing broadband 50 Ω loads at all ports not connected to the VNA, 4 elements of the 16 port S-parameters are defined with each measurement. Because the reflected energy at each port must be measured multiple times, 112 measurements must be taken to completely define the S-parameters of the lens. Using a 4-port VNA the number of measurements is reduced to 35.

Two vector network analysers have been used to measure the performance of the lenses presented in this thesis. The two narrow-band lenses, presented in Section 7.5.1, have been characterised using a two port Wiltron 37369A VNA, calibrated using the Wiltron 3652 calibration kit. The broadband lens, presented in Section 7.5.2, has been measured using a four port Agilent 8364B Performance Network Analyzer (PNA), calibrated using the N4693A 2-port electronic calibration module. All ports not being measured by the VNA have been terminated using Radiall R-404212, DC-18 GHz, 50 Ω loads.

6.3.2 S-Parameter Performance

The electromagnetic simulation package and network analyser measurements generate a set of S-parameters for every frequency point, f, expressed by:

$$\begin{bmatrix} S_{b_1,b_1}(f) & \dots & S_{b_1,b_n}(f) & S_{b_1,a_1}(f) & \dots & S_{b_1,a_m}(f) \\ \vdots & \ddots & \vdots & \vdots & \ddots & \vdots \\ S_{b_n,b_1}(f) & \dots & S_{b_n,b_n}(f) & S_{b_n,a_1}(f) & \dots & S_{b_n,a_m}(f) \\ S_{a_1,b_1}(f) & \dots & S_{a_1,b_n}(f) & S_{a_1,a_1}(f) & \dots & S_{a_1,a_m}(f) \\ \vdots & \ddots & \vdots & \vdots & \ddots & \vdots \\ S_{a_m,b_1}(f) & \dots & S_{a_m,b_n}(f) & S_{a_m,a_1}(f) & \dots & S_{a_m,a_m}(f) \end{bmatrix}. \tag{6.1}$$

The subscripts $b_1 \dots b_n$ refer to each of the n beam ports and $a_1 \dots a_m$ refer to each of the m antenna ports. The various performance measures are obtained directly from Equation (6.1) or calculated, in some part, by evaluating the following equation:

$$\mathbf{b} = \mathbf{S}\mathbf{a}, \tag{6.2}$$

where

$$\mathbf{a} = \begin{bmatrix} a_{b_1}(f) \\ \vdots \\ a_{b_n}(f) \\ a_{a_1}(f) \\ \vdots \\ a_{a_m}(f) \end{bmatrix},$$

$$\mathbf{b} = \begin{bmatrix} b_{b_1}(f) \\ \vdots \\ b_{b_n}(f) \\ b_{a_1}(f) \\ \vdots \\ b_{a_m}(f) \end{bmatrix}.$$

Output Voltage Magnitude Performance

The output voltage magnitude performance is measured by evaluating Equation (6.2) while exciting each beam port in turn. This is achieved by setting $a_{b_x} = 1$ while $a_{b_y} = 0$ for $y \neq x$ and $a_{a_1} \ldots a_{a_m} = 0$. The output voltage magnitude performance is evaluated by examining the magnitudes $b_{a_1}, b_{a_2}, \ldots b_{a_m}$ at each beam port and frequency point.

The lens performance may be evaluated while driving multiple beam ports simultaneously by setting $\mathbf{a}'$ to the required magnitude and setting the total power to 1 using the equation

$$\mathbf{a} = \mathbf{a}' \frac{1}{\sqrt{\sum_{x=1}^{n} |a_{b_x}^2|}}. \tag{6.3}$$

While an ideal lens exhibits a constant excitation taper when driving any single beam port, a realised lens will have considerable difference in excitation taper at different beam ports and frequencies. The shape of the desired excitation taper depends on the intended application. Requirements such as orthogonal beams or maximum power output of an active antenna array require a uniform power distribution across the antenna ports $b_{a_1} = b_{a_1} \ldots = b_{a_m}$. Low sidelobes require an excitation taper that varies significantly from port to port to resemble a sinc or raised cosine function.

Output Phase Performance

The phase performance uses the same procedure used above, except now the phase of $b_{a_1}, b_{a_2}, \ldots b_{a_m}$ is examined. Therefore, the result is expressed by $\theta_{a_1}, \theta_{a_2} \ldots \theta_{a_m}$. The phase gradient across the antenna array determines the direction of the antennas main beam. Any deviation from a linear phase gradient causes the beam pattern to be distorted. This can manifest itself as higher sidelobe or displaced maximum. The ideal phase performance of the Rotman lens, calculated using the geometrical optics model, suggest that the Rotman lens should be capable of driving apertures of ≈ 1000 wavelengths (Rotman and Turner 1963). In practice, the level of performance predicted using the geometrical optics model is not achievable.

Insertion Loss

Insertion loss is easily calculated using the magnitude performance calculated above. Since the total power into the lens has been set to unity, the insertion loss is easily obtained by calculating the total power leaving the antenna ports, $b_{a_1}, b_{a_2}, \ldots b_{a_m}$ using the formula

$$P_{\text{out}} = \sum_{x=a_1}^{a_n} b_x^2. \tag{6.4}$$

The insertion loss is then calculated using

$$\text{Insertion Loss} = -10 \log(P_{\text{out}}).$$

Rotman lenses are often used in applications where conventional beam-forming networks are too lossy to be effective. In these cases insertion loss and port matching are critical to the lens design. The insertion loss of a well matched lens is dominated by the amount of energy absorbed by sidewalls or dummy ports.

Return Loss, Reflection Coefficient, and Array Return Loss

When only one port is excited at any time, or all excitations are considered independent, the *return loss* of each beam port is a simple matter of examining the diagonal components of Equation (6.1). The return loss of the antenna ports, or a multi beam port excitation, is misleading if evaluated in this way since multiple ports are being excited simultaneously. This is because coupled energy between ports may increase or decrease the magnitude of return loss.

To calculate the return loss of port y for a multiple port excitation, the excitation of port y and all others is defined, $\mathbf{a}'$, and normalised using Equation (6.3). The return loss can then be calculated by evaluating

$$\text{Return Loss} = -20\log(b_y)$$

to calculate the return loss. It is generally accepted that return loss should be greater than 10 dB in a well matched system. Return loss is easily confused with *reflection coefficient* which is expressed in dB using

$$\text{Reflection Coefficient} = 20\log(b_y).$$

It is important to emphasise that the return loss for the combined antenna ports is very different depending on the propagating waves incidence angle. The approach adopted is to evaluate the return loss of the antenna ports for incident waves corresponding to each beam port. The return loss of the antenna ports for incident angles away from bore-sight is a significant performance limitation of the Rotman lens. To limit the confusion between the single port return loss and the multi-port return loss, the latter will be referred to as *array return loss*.

Port Isolation, Coupling, Coupling Loss and Reflection Loss

The beam port *isolation*, *coupling*, *coupling loss*, and *reflection loss* are closely related but emphasise different properties. Port coupling describes amount of power coupled between two ports. Port isolation is the minimum attenuation between a port of interest and a defined set of ports. The coupling loss describes how much energy is lost due to coupling between a port of interest and a defined set of ports. The array reflection loss is a term created in this text to describe the energy lost due to reflection from a set of ports when all ports in that set are excited.

The port coupling is the total power exiting a port when a single port or group of sub-ports is excited. The coupling to a port b_y, from an excitation of $\mathbf{a}$ with a total power of 1, is

$$\text{Coupling} = 20\log(b_{b_y}).$$

The beam port isolation is calculated based on the maximum coupling between the beam port of interest and all other beam ports. Therefore, the isolation of port b_y is calculated using

$$\text{Isolation} = 20\log(\max(b_{b_{\ni y}})).$$

The isolation performance is particulary important for systems that are simultaneously transmitting and receiving from different ports of the lens.

The beam port coupling loss is calculated by evaluating

$$P_{\mathrm{b}\ni\mathrm{y}} = -b_{b_y}^2 + \sum_{x=b_1}^{b_n} b_x^2.$$

the coupling loss is then calculated using

$$\text{Coupling Loss} = -10\log(1 - P_{\mathrm{b}\ni\mathrm{y}}).$$

The beam port coupling loss will be similar for all beam ports and tend to effect the low frequency performance of the lens.

The antenna port reflection loss is calculated by evaluating

$$P_{\mathrm{a}_{1\ldots\mathrm{m}}} = \sum_{x=a_1}^{a_m} b_x^2.$$

when all antenna ports are excited and normalised using Equation (6.3). The reflection loss is then calculated using

$$\text{Reflection Loss} = -10\log(1 - P_{\mathrm{a}_{1\ldots\mathrm{m}}}).$$

6.3.3 Beam Pattern Measurement

The Rotman lenses described in Section 7.5.1 are built with an integrated patch antenna array. To characterise the performance of these lenses the beam patterns associated with each beam port are measured using the automated antenna test facility run by the Electronic Warfare and Radar Division of the Defence Science and Technology Organisation in Adelaide. All antenna measurements have been done in accordance with standard practises (IEEE Standard 1979, Beste et al. 1985, Gillespie 1980, Peters 1981).

6.3.4 Beam Pattern Performance

The beam pattern of a lens is obtained by direct measurement, or by applying the results of Equation (6.2) to a theoretical array of real or isotropic elements as described in Section 2.2.2. The primary difference between these two approaches is the effect of mutual coupling between antenna elements of the real antenna array. Like the antenna ports

of the lens, the antenna elements of the array suffer from reflection loss. This reflected energy may degrade the performance of the lens, specifically, the return loss and mutual coupling of the beam ports.

The field-of-view of the lens is often the first requirement defined in the lens specification. The design challenges grow as the desired field-of-view increases due to mutual coupling of the antenna ports. While the beam associated with the central focal point of the lens tends to perform well for all practical lens designs, it it the performance of the outermost beams that will be significantly degraded. The 3 dB field-of-view of the lens is the maximum scan angle that is achievable before the insertion loss of the lens drops by 3 dB below the lens's minimum insertion loss.

6.4 Chapter Summary

This chapter has described the tools used in this work to design, build and characterise the lenses presented in this thesis. Matlab is used to conduct all numerical analysis of the lens designs. Matlab has also been used to create a custom layout tool capable of exporting the lens designs to DXF or Gerber format. Electromagnetic simulation is carried out using Ansoft Designer, or its predecessor Ansoft Ensemble, and HFSS. The equipment and procedures used to measure S-parameters and beam patterns of the three lens designs has also been described. Finally each performance measure used to compare the measured and simulated results has been explained.

The following chapter focuses on the practical implementation of the Rotman lens. The electromagnetic performance of the port to lens interface is explored and new matching techniques are described. Finally the methods presented in this chapter are applied to two narrow-band lens designs in Sections 7.5.1 and 7.5.1 and a broadband lens design in Section 7.5.2.